Soft Matter

PAPER

View Article Online
View Journal | View Issue

Check for updates

Cite this: *Soft Matter*, 2018, **14**, 4591

Processing of PVDF-based electroactive/ferroelectric films: importance of PMMA and cooling rate from the melt state on the crystallization of PVDF beta-crystals†

Alexandre De Neef,[abc] Cédric Samuel,[*bc] Grégory Stoclet,[cd] Mohamed Rguiti,[e] Christian Courtois,[e] Philippe Dubois,[a] Jérémie Soulestin[bc] and Jean-Marie Raquez[a]

Poly(vinylidene difluoride) (PVDF) displays attractive ferroelectric/piezoelectric properties and its polar β-crystals are specifically targeted for achieving electroactive applications. However, their direct crystallization from the melt state represents a challenging task that has never been addressed using melt-state processes. The use of poly(methyl methacrylate) (PMMA) is herein investigated to promote the PVDF polar β-phase using melt-blending and extrusion–calendering technologies. The presence of the β-phase is here confirmed by ATR-FTIR and WAXS experiments with blends at a PMMA content as low as 5 wt%. The key role of PMMA for the β-phase crystallization from the melt state was unambiguously highlighted with the help of Flash DSC experiments in non-isothermal cooling mode from the melt state. PMMA is able to efficiently shift the α-to-β crystal transition to lower cooling rates (>100–200 °C s^{-1}), making the achievement of the PVDF polar β-phase for these blends compatible with conventional processing tools. A crystal phase diagram is proposed for the PVDF/PMMA blends to highlight the dual effects of both PMMA and cooling rate on the PVDF crystallization during melt-processing. Ferroelectric properties were even observed for the blends containing PMMA up to 10 wt% with the highest remanent polarization obtained at 5 wt% PMMA. After 10 wt% PMMA, a progressive transition from ferroelectric to pseudo-linear dielectric behavior is observed more likely due to the presence of PMMA in the interlamellar amorphous phase of the polar PVDF spherulites as shown by SAXS experiments. In this work, we successfully demonstrated that PMMA plays a key role in the crystallization of PVDF polar crystals from the melt state, enabling large-scale and continuous extrusion processing of PVDF-based materials with attractive dielectric properties for sensing and harvesting applications.

Received 6th February 2018,
Accepted 13th April 2018

DOI: 10.1039/c8sm00268a

rsc.li/soft-matter-journal

Published on 16 April 2018. Downloaded by Michigan State University on 8/13/2019 12:24:31 PM.

Introduction

Fluoropolymers such as poly(vinylidene difluoride) (PVDF) and their related copolymers represent a unique class of polymer materials with attractive ferroelectric, piezoelectric and electroactive properties.[1–3] These polymers can find numerous applications like as sensors and transducers and even for future applications in microelectronics, robotics and energy with the development of flexible sensors, actuators, piezoelectric energy harvesters, random-access memories and self-charging batteries.[2,4–6]

The elevated electroactive properties of PVDF arise from the high dipolar moment of the vinylidene difluoride (VDF) unit, combined with some specific chain conformations in the crystalline lattice.[7] PVDF-based polymers are semi-crystalline with a very high crystallinity extent up to 54%,[8] and four distinct crystalline phases of different chain conformations can be observed,[2] *i.e.* the β-phase (chain configuration 100% *trans*), the α-phase (configuration TGTG′), the δ-phase (similar chain conformation than α-phase)[9] and the γ-phase (configuration T_3GT_3G'). Each crystalline phase presents a specific dipole moment (generated by the difference of electronegativity between the fluorine atoms and hydrogen/carbon atoms) with variable dipolar contribution per unit cell,[10] spanning between 0 and 8×10^{-30} C m for the α-phase and β-phase, respectively. Therefore, the polar β-phase of

[a] *University of Mons (UMons), Laboratory of Polymeric and Composite Materials (LPCM), Center of Innovation and Research in Materials and Polymers (CIRMAP), Place du Parc 23, B-7000 Mons, Belgium*
[b] *Ecole Nationale Supérieure Mines Telecom Lille Douai, Institut Mines Telecom Lille Douai (IMT Lille Douai), Département Technologie des Polymères et Composites & Ingénierie Mécanique (TPCIM), 941 rue Charles Bourseul, F-59508 Douai, France. E-mail: cedric.samuel@imt-lille-douai.fr*
[c] *Université de Lille, F-59000 Lille, France*
[d] *Université de Lille, CNRS INRA ENSCL UMR 8207 Unité Matériaux et Transformations (UMET), F-59000 Lille, France*
[e] *Université de Valenciennes, EA 2443 Laboratoire des Matériaux Céramiques et Procédés Associés (LMCPA), F-59313 Valenciennes, France*

† Electronic supplementary information (ESI) available. See DOI: 10.1039/c8sm00268a

Published on 16 April 2018. Downloaded by Michigan State University on 8/13/2019 12:24:31 PM.

PVDF is preferred to design electroactive PVDF-based materials with the highest ferroelectric/piezoelectric properties. Spontaneous/remanent polarization in the range 6.5–9 μC cm^{-2} and d_{31}/d_{33} piezoelectric coefficients close to 25–35 pC N^{-1} [2,3,11–15] can be reached with such PVDF. However, the processing of PVDF into the polar β-phase is not straightforward. In order to obtain the β-phase from neat PVDF, three processing methods have been reported such as the use of high pressure crystallization (>700 MPa), fast quenching from the melt state (>2000 °C s^{-1}) and stretching from the rubbery state under specific conditions (close to 80 °C up to a stretching ratio of 5).[2] This popular stretching approach enables the α-phase to be converted into the β-phase (approx. 20% of α-phase remaining), leading to interesting piezoelectric/ferroelectric properties after an adequate high-voltage poling step.[3,11,14,15] However, in view of industrial implementation, the direct recovery of the PVDF β-phase from the melt state still represents a challenging task and other strategies have been thereby developed.

Among them, copolymerizing VDF with trifluoroethylene comonomer (TrFE) gives access to the so-called poly(vinylidenefluoride-*co*-trifluoroethylene) (PVDF-TrFE) copolymers with attractive electroactive properties.[1,2] Such copolymerization makes it possible to get the direct recovery into the crystalline β-phase at the expense of the α-phase, independently of the processing method.[2,16] The accepted mechanism for β-phase formation in PVDF-TrFE involves the chain-torsion by the introduction of bulky additional F atoms from the TrFE unit, resulting in an energetically favored 100% *trans* conformation. A good ferroelectric behavior is so-observed with spontaneous/remanent polarization (P_r) and piezoelectric coefficient d_{33} up to 11 μC cm^{-2} and −38 pC N^{-1}, respectively.[2,16,17] Varying the amount of TrFE comonomer within PVDF-TrFE makes it possible to tune their ferroelectric and relaxor behaviors. However, melt-processing of PVDF-TrFE is relatively limited by the cost of these copolymers and solvent-processing is preferred to produce devices from these materials. The decrease of the Curie temperature (ferroelectric/paraelectric transition) after copolymerization remains the main issue, restricting their utilization to low temperature applications (<80 °C).[2,16] The polar β-phase of neat PVDF can also be obtained after the introduction of various nanoparticles such as carbon nanotubes, palladium, ferrite, and $BaTiO_3$ nanoparticles.[18–20] In the case of carbon nanotubes, the β-phase is even observed with only 0.01 weight% of CNTs. Unfortunately, CNTs can create an electrical percolation pathway within the PVDF nanocomposite,[21] making the PVDF poling step under high electric field extremely difficult.[22]

The most interesting approach to achieve a direct recovery of the PVDF β-phase from the melt state appears to be *via* melt-blending PVDF with (partially-)miscible polymers. This route represents a promising and cost-competitive approach for producing films and fibers at an industrial level. Some (partially-)miscible polymers such as poly(methacrylate) can even modify the PVDF crystallization behavior and promote the PVDF β-phase crystallization. Indeed, the miscibility between poly(methyl methacrylate) (PMMA) and PVDF with related ferroelectric/piezoelectric characterization has been intensively studied and reviewed.[1,12,17,23–28] The direct β-phase formation from the melt state was first demonstrated by Léonard C. and coworkers.[26] The amount and tacticity of PMMA seems to play a key role in the PVDF crystallization and the authors also postulated that the resulting PVDF crystalline phase could be governed by the crystallization temperature as a function of the cooling rate from the melt. They have also demonstrated the occurrence of specific H-bonding interactions between $-CH_2$ groups of PVDF and carbonyl groups of PMMA that could increase of the amount of *trans* sequence of PVDF segments. Similar results were also reported by Domenici C. *et al.* with the incorporation of 30 wt% of PMMA into PVDF using a solvent-based approach. However, in terms of ferroelectric/piezoelectric properties, contradictory results have been reported so far. Most of the authors reported that the spontaneous/remanent polarization, the coercitive field and the piezoelectric coefficients decrease with the amount of PMMA.[12,17,28] In contrast, Li *et al.* proved that PVDF/PMMA blends could be competitive enough with PVDF-TrFE, especially for high temperature applications with stable ferroelectric properties up to 120 °C at least. In a recent investigation, the dielectric behavior of PVDF-TrFE was readily tuned by the incorporation of miscible grafted poly(methacrylates).[29] Ferroelectric, anti-ferroelectric, relaxor to linear dielectric behavior was demonstrated by playing with the miscibility extent, leading to a "nanoconfinement" of PVDF β-crystals. All these previous findings proved that these miscible PVDF/PMMA blends could represent promising materials with controllable properties but the mechanism behind the direct crystallization into the polar β-phase for these PVDF/PMMA miscible blends is lacking and needs to be investigated using both adequate processing conditions and optimized PMMA content. Within this research framework, advanced calorimetry techniques represent an efficient way to perfectly highlight these important features and especially the effect of the cooling rate. Recently, the crystallization of neat PVDF was investigated at high cooling rates *via* Flash-DSC techniques. The authors highlight a crystal modification at high cooling rates.[30–33] The β-phase crystallization at a high cooling rate is still controversial, but this important finding means that the crystallization mechanisms of PVDF into the β-phase could be controlled from the melt state with the cooling rate.[33] To the best of our knowledge, the PMMA effect on the crystallization of PVDF at high cooling rates is still unknown, together with the fact that the use of miscible partners such as PMMA may lead to counter-intuitive effects on crystallization, especially in the crystal nucleation phase.[34]

In an effort to produce electroactive polymer films using continuous extrusion processes, the present study will focus on the role of PMMA regarding the crystallization extent of polar PVDF β-crystals from the melt state. Several melt-based techniques (extrusion–calendering *vs.* thermocompression) were compared for their crystallization ability of PVDF-based blends at various PMMA contents by means of WAXS and FTIR techniques. A deep insight over the role of PMMA in the crystallization of the PVDF polar β-phase was obtained through Flash DSC experiments to achieve cooling rates as high as 3000 °C s^{-1} and get representative information on the crystallization of PVDF/PMMA blends during

 This journal is © The Royal Society of Chemistry 2018

Published on 16 April 2018. Downloaded by Michigan State University on 8/13/2019 12:24:31 PM.

film extrusion processing. A crystal phase diagram was attempted and discussed as well as the ferroelectric performances of the final PVDF/PMMA films as produced by extrusion–calendering.

Experimental section

Materials

Poly(vinylidene difluoride), hereafter called PVDF, was kindly supplied by Arkema (grade Kynar® 720, M_w = 200 000 g mol^{-1}). Poly(methyl methacrylate), hereafter called PMMA, was supplied by Evonik (grade 8N, M_w = 97 000 g mol^{-1}). Throughout this contribution, all percentages are given as weight percentage (wt%).

Film extrusion–calendering

The first processing method for PVDF/PMMA miscible blends is the film extrusion–calendering as described by Leveque *et al.*[35] In the first step, PVDF and PMMA formulations were melt-blended in a co-rotating twin-screw extruder (Haake Rheomex PTW 16 OS, ThermoScientific, Germany) with a screw diameter of 16 mm for a L/D ratio of 40. Extrusion temperatures were set to 210 °C (except for the temperature of the extrusion die set at 170 °C). PVDF and PMMA pellets were dry-blended, extruded (screw speed between 150 and 200 rpm, mass flow rate between 1 and 1.2 kg h^{-1}) and pelletized. The as-produced PVDF/PMMA pellets were reprocessed by film extrusion–calendering with a Haake single screw extruder with an L/D ratio equal to 40, a temperature profile of 170–210–210–230 °C (from the hopper to the die) and a screw speed of 60 rpm. The extrusion die consists of a specific slit die for film extrusion (width 150 mm, thickness 800 μm) and the film extrudate was subsequently calendered to obtain 20–120 μm-thick films. The calendering system is equipped with a cooling system using cold water (10 °C) within the compression cylinders (estimated cooling rate ±200 °C s^{-1} according to expected thickness).

Thermocompression molding

The extrusion/thermocompression process is described by Samuel *et al.*[34] PVDF and PMMA were blended in an internal mixer Brabender at 210 °C and 75 rpm for 10 min. The collected melt-blends were subsequently molded into thin films using a Carver press at 210 °C and 10 bars for 1 min (after melting and conditioning). Then, the samples were quenched from the melt state using a cold water flow until reaching a temperature at 20 °C (estimated cooling rate ±1 °C s^{-1}).

Flash differential scanning calorimetry (FDSC)

FDSC experiments were carried out on a Mettler-Toledo Flash DSC[36] *via* a specific protocol to observe the crystallization extent at different cooling rates. The measuring cell was continuously flushed with nitrogen gas and high-purity indium was used for temperature calibration of the sensor. A sample of about 35–100 ng was placed under a microscope on the active area of the circular 500 μm-diameter sensor. The procedure used for crystallization analyses is the following: heating at 1000 °C s^{-1} to 210 °C, isotherm at 210 °C during 10 s, cooling at controlled cooling rates between −5 °C s^{-1} and −4000 °C s^{-1} to −80 °C, isotherm at −80 °C during 10 s, heating at 5000 °C s^{-1} to 210 °C s^{-1}. This procedure was repeated at different cooling rates as shown in Fig. 1. Crystallization temperatures (T_c) were determined at the maximum of the exothermic peak observed during the cooling scan. For the sake of clarity, cooling curves were normalized by the heating rate. Note that the sample mass used for FDSC was approached by measuring crystallization/melting enthalpies at low cooling/heating rates (1 °C s^{-1}) using a classical Mettler Toledo DSC1.

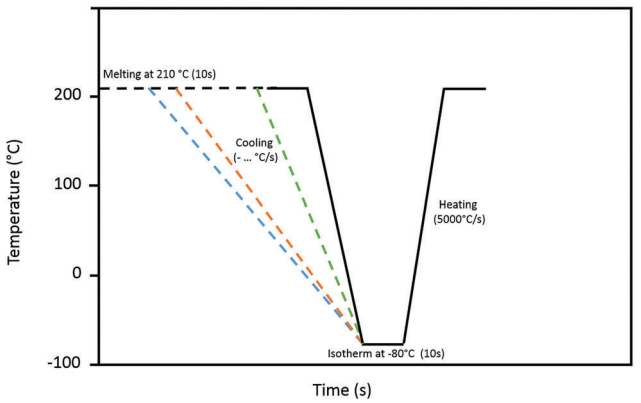

Fig. 1 Temperature–time profiles used to investigate the crystallization for PVDF/PMMA blends during high-speed cooling by Flash DSC. The samples were characterized at different cooling rates between −5 °C s^{-1} and −3000 °C s^{-1} from the melt state followed by a melting step at high heating rate.

Attenuated total reflection–Fourier transform infrared spectroscopy (ATR-FTIR)

Crystal phases of PVDF/PMMA blends were identified by Fourier transform infrared spectroscopy (FTIR) using a BIO-RAD Excalibur spectrometer equipped with an ATR Harrick Split Pea™ apparatus from SAFIR Cie. Spectra were recorded using a spectral width ranging from 550 to 1400 cm^{-1} with 4 cm^{-1} resolution and an accumulation of 32 scans.

Wide angle and small angle X-ray scattering (WAXS & SAXS)

Wide Angle X-ray Scattering (WAXS) and Small Angle X-ray Scattering (SAXS) analyses were carried out at room temperature in transmission mode on thin PVDF/PMMA films. The analyses were performed on a Xeuss apparatus (Xenocs, France) and the CuKα radiation (l = 1.54 Å) was used. The sample to detector distance was set at 10 cm and 1 m for the WAXS and SAXS experiments respectively and calibrated thanks to a Silver Behenate sample. The WAXS and SAXS patterns were recorded on a Pilatus detector (Dectris). The intensity profiles were obtained by 360° azimuthal integration of the 2D patterns using the Foxtrot software®. It was used to determine the crystalline composition of the PVDF-based blends. The diffraction spectra were measured at an angle value (2θ) between 5 and 30°.

Polarized light optical microscopy (PLOM)

Crystalline morphologies were observed by polarized light optical microscopy using a Leica DM 2500M microscope

Published on 16 April 2018. Downloaded by Michigan State University on 8/13/2019 12:24:31 PM.

(magnification ×20) equipped with a Mettler FP82 hot-stage apparatus and Mettler FP80 microprocessor. Briefly, extruded films were melted between two glass plates at 210 °C for about 10 min. Then, the samples were cooled using various procedures to observe the development of crystalline structures. Images were then treated by image anlysis using ImageJ software to evaluate the crystal densities from micrographs.

Ferroelectric analysis

P–E hysteresis loops were obtained by a Radiant Precision Workstation ferroelectric testing system at room temperature equipped with a high-voltage source of 10 kV. The Vision5 data management software were used to obtain the results at a frequency of 1 Hertz with the normal dipolar mode, which produced a triangular signal of high voltage and made it possible to measure the subsequent polarization of the PVDF/PMMA films.

Results and discussion

The direct crystallization of PVDF/PMMA into the polar β-phase was first investigated on thin films produced by solvent-free processes. Thin films of thickness lower than approx. 100 μm are preferred for electroactive applications to avoid excessive electric fields during high-voltage poling[37] and two sets of experiments were performed. Films were manufactured by either a continuous extrusion–calendering process or a discontinuous thermo-compression process to get a clear comparison between both processes in terms of PVDF crystallization and ferroelectric properties. The PMMA weight ratio within the PVDF/PMMA blends was progressively increased (PVDF/PMMA 100 : 00, 95 : 05, 90 : 10, 80 : 20 and 70 : 30) to observe the evolution of crystalline phases as a function of the PMMA content. The characterization of the PVDF crystalline phases for each formulation and process was systematically performed using ATR-FTIR and WAXS techniques. ATR-FTIR makes it possible to identify the crystalline phases of PVDF with the characteristic absorption peaks for the α-phase (766 and 795 cm^{-1}) and the β-phase (840 cm^{-1}).[38] It could be noticed that other PVDF crystalline phases such as γ-phase had absorption peaks close to that of the β-phase[2] and ATR-FTIR could not easily resolve between these two phases. PMMA also presents similar absorption peaks to those of PVDF as demonstrated by Vietmann *et al.*[39] In this respect, WAXS analyses are needed to distinguish the PVDF crystalline phase between the crystalline lattices related to the α-phase (2θ = 18.3°, 19.9° and 26.6°) and β-phase (2θ = 20.3°).[40] Fig. 2 and 3 show ATR-FTIR and WAXS characterization, respectively, for both extrusion–calendered (thickness ±60 μm) and thermocompressed blends. For neat PVDF, both processing methods give similar ATR-FTIR and WAXS patterns. ATR-FTIR absorption peaks close to 765 and 795 cm^{-1} are observed (Fig. 2a and b). WAXS diffraction peaks at 2θ angles close to 18.5, 20.0 and 26.5 cm^{-1} are in agreement with the ATR-FTIR results (Fig. 3a and b) and confirmed the presence of the crystalline α-phase in all neat PVDF films. No significant trace of the β-phase is detected by WAXS and ATR-FTIR techniques. These observations on PVDF films produced by either extrusion–calendering or thermo-compression are in agreement with the state of the art, reporting the presence of a quasi-pure non polar α-phase. The incorporation of PMMA clearly modifies the crystalline phase of PVDF and both processes produce different trends in terms of PVDF crystalline phases. In the case of an extrusion–calendering process, the apparition of the β-phase at 840 cm^{-1} is clearly detected using a PMMA content as low as 5 wt%, with a simultaneous decrease of absorption peaks related to the α-phase (Fig. 2a). Between 5 and 10 wt% PMMA, the α-phase and β-phase of PVDF both coexist after extrusion–calendering and the α-phase totally disappears at 20 wt% PMMA. WAXS patterns for extrusion–calendered films also display a similar trend (Fig. 3) with the apparition of a small shoulder at 20.5° at 5 wt% PMMA. Some slight differences from the ATR-FTIR results could be ascribed to the crystal size effects. The β-phase is also observed for PVDF/PMMA films produced by thermocompression, but 25–30 wt% PMMA is required to obtain the polar β-phase as observed by ATR-FTIR and WAXS techniques (Fig. 2b and 3b). This result obtained for the thermocompression process of PVDF/PMMA blends is consistent with the previous studies reported in the litterature.[23,41–43] As a first conclusion, PMMA clearly promotes

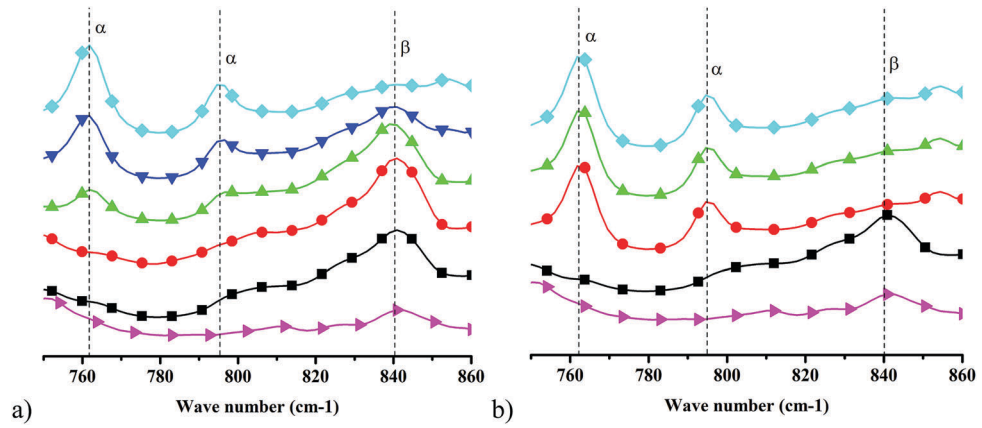

Fig. 2 ATR–FTIR analysis of neat PVDF (-♦-), PVDF/PMMA 95 : 5 (-▼-), PVDF/PMMA 90 : 10 (-▲-), PVDF/PMMA 80 : 20 (-●-), PVDF/PMMA 70 : 30 (-■-) and neat PMMA (-►-) blends obtained by extrusion–calendering (a) or by thermo-compression (b) (film thickness *ca.* 60 μm).

 This journal is © The Royal Society of Chemistry 2018

Published on 16 April 2018. Downloaded by Michigan State University on 8/13/2019 12:24:31 PM.

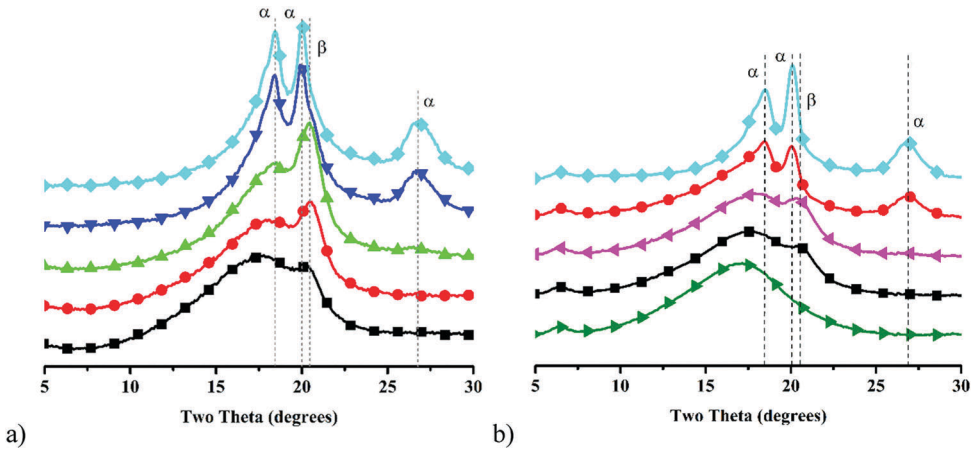

Fig. 3 WAXS analysis of neat PVDF (-♦-), PVDF/PMMA 95 : 5 (-▼-), PVDF/PMMA 90 : 10 (-▲-), PVDF/PMMA 80 : 20 (-●-), PVDF/PMMA 75 : 25 (-◀-), PVDF/PMMA 70 : 30 (-■-) and PVDF/PMMA 60 : 40 (-▶-) blends obtained by extrusion–calendering (a) or by thermo-compression (b) (film thickness *ca.* 60 μm).

the PVDF β-phase for both processes, but it can be readily obtained at a very low amount of PMMA close to 5 wt% using the extrusion–calendering process in order to produce PVDF polar crystals. It could also be noticed that the presence of the PVDF γ-phase is also clearly discarded in our formulations and processing conditions based on the absence of its characteristic absorption peak at 1234 cm^{-1} (ESI,† Fig. S01).

The influence of the film thickness has a significant practical importance for further production of electroactive PVDF/PMMA films. It is worth mentioning that lower voltages are required for the poling process in the case of ultra-thin films. In this respect, additional experiments were performed by extrusion–calendering. The film thicknesses were varied from 200 μm to 20 μm for neat PVDF and PVDF/PMMA 95 : 5 films. Interestingly, neat PVDF films with thicknesses lower than 60 μm could present a low amount of polar β-phase by extrusion–calendering as observed by ATR-FTIR with the presence of a small and broad absorption peak at 840 cm^{-1} (Fig. 4a). A similar effect is also observed for the PVDF/PMMA 95 : 5 films (Fig. 4b). The signal intensity at 840 cm^{-1} related to the β-phase progressively increases with decreasing film thickness and the signal intensities related to the α-phase are simultaneously decreasing. The relative amount of β-phase over α-phase could be enhanced by manufacturing thin PVDF/PMMA films of thicknesses as low as 20 μm, even for neat PVDF. A high β-phase content could be achieved by tuning the processing conditions (PMMA content, film thickness and processing method) but quantitative information about crystallization with a special emphasis on related mechanisms is clearly compulsory for further material/process optimization.

The β-phase formation in a miscible PVDF/PMMA blend was previously observed using other production processes and the quenching temperature from the melt state was identified as a key parameter for β-phase recovery.[17,28,44–46] A cooling rate effect was also mentioned by Léonard *et al.* to explain PVDF crystal modifications at a PMMA content between 20 and 30 wt% but no experiments were actually performed to confirm the role of cooling rate.[26] Thermocompression and extrusion–calendering processes significantly differ in terms of cooling rate (1 °C s^{-1}

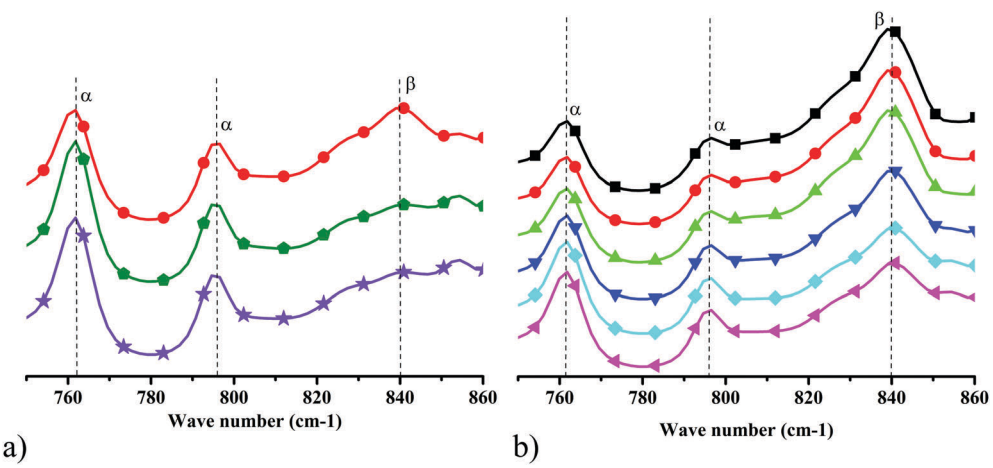

Fig. 4 FTIR analysis of neat-PVDF (a) and PVDF/PMMA 95 : 5 (b) at different thicknesses, 200 μm (-◀-), 120 μm (-♦-), 100 μm (-*-), 80 μm (-▼-), 60 μm (-⬠-), 40 μm (-▲-), 30 μm (-●-) and 20 μm (-■-), obtained by extrusion–calendering.

Published on 16 April 2018. Downloaded by Michigan State University on 8/13/2019 12:24:31 PM.

for thermocompression *vs.* 10–500 °C s^{-1} for extrusion–calendering)[47] and a synergistic effect between PMMA and the cooling rate on the β-phase production could be here speculated to consolidate the actual and previous results. However, the efficiency of the extrusion–calendering process to induce PVDF polar β-crystals at low PMMA content and low film thickness could also be interpreted in terms of induced orientation by uniaxial stretching in the melt state at the die, having likely an impact on the PVDF β-phase recovery. In this context, various experiments were conducted to evaluate the residual orientation of the PVDF/PMMA films. The orientation of the crystalline domains was first investigated by WAXS after extrusion–calendering (ESI,† Fig. S02). A slight orientation of the α-phase and β-phase is detected along the stretching axis but no correlation with PMMA content is obtained. The quantitative analysis indicates a poor orientation with P_2-factor comprised between 0 and 0.1. Concerning the amorphous phase, shape variations after reheating to 100 °C were recorded (ESI,† Table S01) but no shape changes were again detected up to 2 hours. In this context, it can be confidently concluded that the uniaxial stretching in the melt state by extrusion–calendering does not induce any orientation, and therefore the orientation effects on the β-phase production can be ruled out. In an effort to identify a combination between PMMA and the cooling rate on β-phase production from an unoriented melt state, PVDF/PMMA thin films were (re)melted at 210 °C followed by a quenching stage to various temperatures using liquid nitrogen (LN_2) (−196 °C), LN_2/methanol (−80 °C), cold water (0 °C) and temperate water (35 °C). ATR-FTIR spectra are gathered in the ESI,† Fig. S03. The PMMA contents required for the β-phase appearance ($X_{PMMA\text{-}\beta\text{-}start}$) and α-phase extinction ($X_{PMMA\text{-}\alpha\text{-}end}$) are listed in Table 1 for all quenching media and techniques. High efficiencies are observed using cold water or LN_2/methanol quenching media with significant amounts of polar β-crystals produced in neat PVDF and total extinction of the α-phase at a PMMA content as low as 10 wt%. Decreasing quenching efficiencies in the order cold water > LN_2/methanol > extrusion–calendering > LN_2 > temperate water 35 °C > thermocompression are observed and confirmed the key role of the cooling rate in the β-phase recovery. A counter-intuitive result is however obtained with an LN_2-containing medium that could be related to poor heat transfer exchange and explained by the intense LN_2 evaporation at the molten film surface. Interestingly, the extrusion–calendering technique with quenching performed at approx. 10 °C on a rotative metal roll displays an intermediate quenching efficiency between cold water (0 °C) and mild water (35 °C) for the PVDF crystal transitions. Consequently, from all the above results, it could be stated that (i) the stretching in the melt state during extrusion–calendering has a low influence on the β-phase production and (ii) the α-to-β crystal transition in PVDF is controlled by the cooling rate applied and the amount of PMMA incorporated.

Table 1 Estimated PMMA content required for the β-phase appearance ($X_{PMMA\text{-}\beta\text{-}start}$) and α-phase extinction ($X_{PMMA\text{-}\alpha\text{-}end}$) as a function of the quenching temperature/method from the melt state

Quenching temperature/method	$X_{PMMA\text{-}\beta\text{-}start}$ (wt%)	$X_{PMMA\text{-}\alpha\text{-}end}$ (wt%)
Thermocompression	25	30
Extrusion–calendering	5	10
LN_2	10	20
LN_2/methanol	0	15
Cold water (0 °C)	0	10
Mild water (35 °C)	15	20

To demonstrate both effects of the PMMA content and the applied cooling rate, and more particularly to obtain quantitative information (crystallization temperature, crystallization rate, *etc.*) about β-phase crystallization from an unoriented molten PVDF/PMMA blend, differential scanning calorimetry (DSC) techniques are of high interest in this case. However, given the use of high cooling rates during the β-phase recovery, the fast scanning DSC techniques represent the most adequate tool to study the crystallization of such fast-crystallizing polymers like PVDF under cooling conditions similar to those used during processing. Flash DSC can highlight the crystallization behaviors under drastic cooling conditions up to 5000 °C s^{-1} and several fundamental pieces of information about the crystallization steps/mechanisms can be obtained.[48–50] In particular, several authors already investigated the crystallization behavior of PVDF by Flash DSC.[32,33,51,52] An obvious change in the crystallization behavior was observed at high cooling rates but controversial conclusions were stated. Neat PVDF was herein subjected to Flash DSC experiments with the procedure displayed in Fig. 1. Crystallization endotherms were recorded at various cooling rates, ranging from 80 to 3000 °C s^{-1} (Fig. 5a). For cooling rates lower than 300 °C s^{-1}, a single crystallization exotherm is detected in the range 100–80 °C. Knowing that the α-phase appears spontaneously for PVDF by conventional processing conditions, we can confidently assume that the single crystallization peak at low cooling rates is ascribed to the PVDF α-phase. Higher cooling rates are marked by the apparition of a second distinct exotherm at lower crystallization temperatures and this second exotherm becomes predominant at cooling rates higher than 1000 °C s^{-1}. Our results are in agreement with previous ones from the literature and correlations with our extrusion–calendering experiments obviously demonstrate the crystal transition from α-phase to β-phase at high cooling rates for neat PVDF, hereafter called the α-to-β crystal transition. A α/β-phase co-crystallization occurs at cooling rates between 400 and 1200 °C s^{-1} for neat PVDF. It could be noticed that the high cooling rate required to develop a pure β-phase for neat PVDF is difficult to achieve in any industrial process and only a partial crystallization extent seems to be more realistic like in the case of our extrusion–calendered neat PVDF thin films. The cooling rate has a major influence on the crystallization of the polar β-phase for neat PVDF and it is also of high interest to determine the impact of PMMA on the α-to-β transition. PVDF/PMMA blends with 5, 10 and 20 wt% of PMMA were subsequently subjected to Flash DSC experiments (Fig. 5b and c) using similar procedures to those exposed in Fig. 1. PVDF/PMMA blends also display similar trends to neat PVDF with the α-phase crystallization at low cooling rates followed by the characteristic α/β co-crystallization at intermediate cooling rates (Fig. 5b and c).

 This journal is © The Royal Society of Chemistry 2018

Published on 16 April 2018. Downloaded by Michigan State University on 8/13/2019 12:24:31 PM.

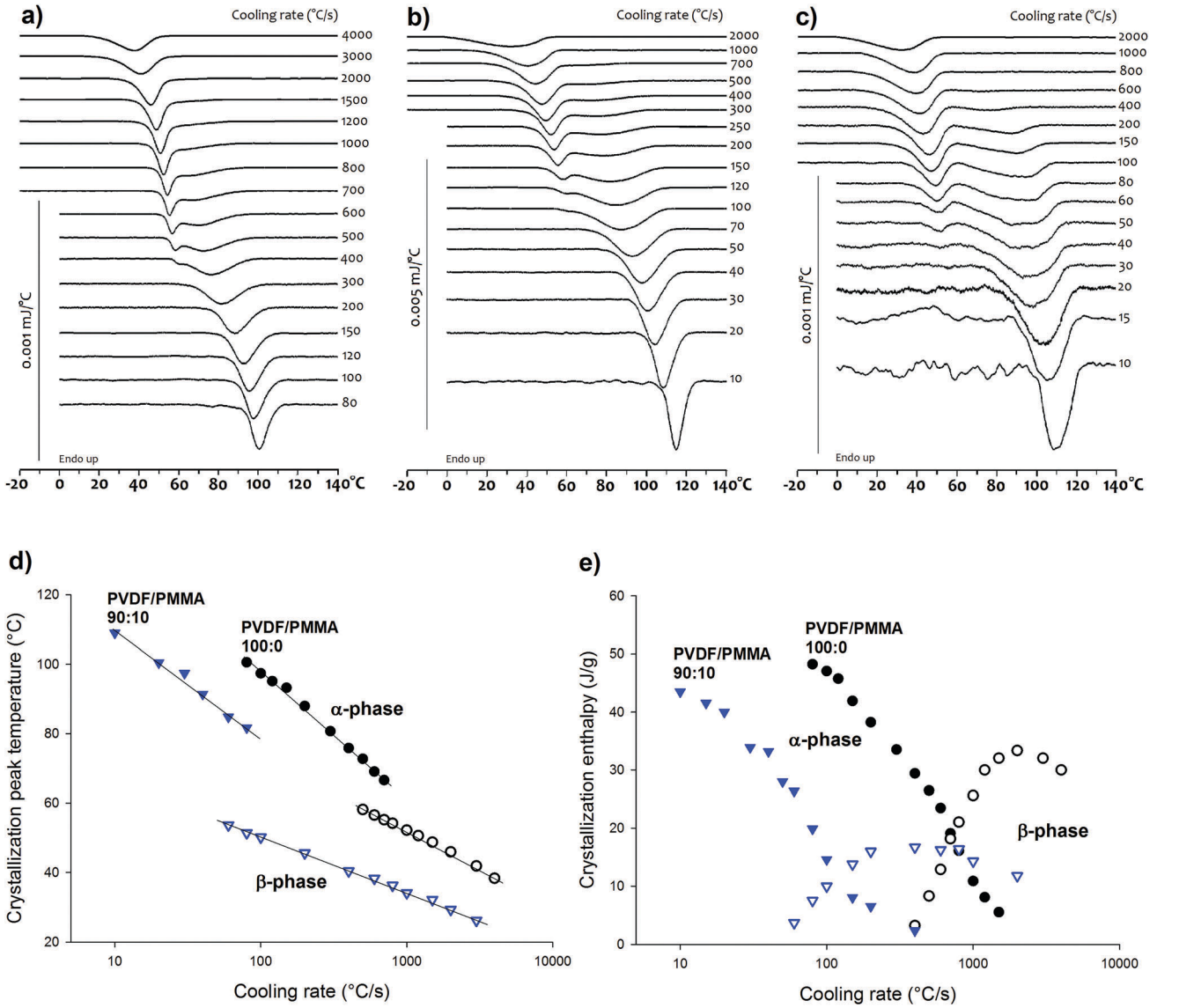

Fig. 5 Cooling scans by FDSC at various cooling rates for neat PVDF (a), PVDF/PMMA 95 : 5 (b), PVDF/PMMA 90 : 10 (c), and PVDF/PMMA 80 : 20 (d). Related crystallization temperatures (d) and crystallization enthalpies (e) for the α-phase and β-phase as a function of cooling rate.

In addition, PMMA induces drastic changes in terms of cooling rates required to develop the polar β-phase and the related diminishing of the α-phase. Concerning the PVDF/PMMA blend at 5 wt% PMMA, the β-phase crystallization starts at a lower cooling rate than neat PVDF (100 °C s^{-1} *vs* 400 °C s^{-1} respectively) and the α-to-β transition is observed in the range 100–800 °C s^{-1}, compared to 400–1200 °C s^{-1} for neat PVDF. This range again decreases at 10 wt% PMMA to reach approx. 50–600 °C s^{-1}. FDSC consequently highlights that (i) the cooling rate from an unoriented melt state represents a key factor to convert non-polar α-crystals into polar β-crystals for either neat PVDF or PVDF/PMMA blends and (ii) the addition of PMMA efficiently shifts the PVDF α-to-β crystal transition to lower cooling rates. Note that such cooling rates are potentially achievable with some classical extrusion tools and technologies, as discussed hereafter.

The crystallization temperatures of the PVDF α-crystals and β-crystals with related enthalpies could be extracted from FDSC cooling traces and their respective evolutions with the cooling rate are displayed in Fig. 5d and e for neat PVDF and the PVDF/PMMA 90 : 10 blend. In the first approach, the evolution of the crystallization temperatures highlights the α-to-β crystal transition with the α-phase crystallization at low cooling rates (high crystallization temperatures) and the β-phase crystallization at high cooling rates (low crystallization temperatures) (Fig. 5d). It could be observed that, at a constant cooling rate, the α- and β-phase crystallization temperatures clearly shift to lower temperatures with the incorporation of 10 wt% PMMA (Fig. 5d). The crystallization enthalpy related to the α-phase continuously drops for neat PVDF and PVDF/PMMA 90 : 10 blends by increasing the applied cooling rate (Fig. 5e). In the meantime, the crystallization enthalpy related β-phase starts to increase until a maximum is

Published on 16 April 2018. Downloaded by Michigan State University on 8/13/2019 12:24:31 PM.

reached followed by its own disappearance at extreme cooling rates. Note that the optimum cooling rate for a maximal β-phase crystallization rate could be evaluated to 350–400 and 2000 s^{-1} for PVDF/PMMA 90 : 10 and neat PVDF respectively. The crystallization enthalpy is significantly lower in the case of the PVDF/PMMA 90 : 10 blend than that of neat PVDF with a quasi-amorphization at high cooling rates. A total amorphization over the entire FDSC cooling rate range is observed for the PVDF/PMMA blend with 20 wt% PMMA (ESI,† Fig. S03). PMMA consequently induces a high depression of all crystallization temperatures and crystallization rates within the entire FDSC cooling rate range independently of the crystal type. These phenomena are largely attributed to the miscibility of PVDF/PMMA with a well-known inhibition of the PVDF crystallization.[23,53–55] Interestingly, the β-phase crystallization clearly proceeds at low temperatures typically between 55 and 25 °C by using high cooling rates that inhibit the α-phase crystallization. Crystallization of the β-phase is also possible at very low temperatures (15 °C) with reduced rates as revealed by annealing experiments of the amorphous PVDF/PMMA 80 : 20 at low cooling rates (ESI,† Fig. S03). We suspected that these behaviors could be related to the crystal nucleation process, *i.e.* a heterogeneous nucleation promoted by impurities for the α-phase[51] and a low-temperature homogeneous nucleation for the β-phase. Such effects could be supported by recent FDSC studies on several semi-crystalline polymers such as poly(amide),[56] poly(propylene)[31] or poly(L-lactide acid)[30] at high cooling rates. For this purpose, microscopic observations are of great importance to evaluate the crystal/nuclei density under large undercooling.[57] In this context, PLOM experiments were performed on PVDF/PMMA 90 : 10 thin films (ESI,† Fig. S04). Two different thermal treatments from the melt state were applied, *i.e.* a cooling step at 10 °C min^{-1} and a quenching step into cold water (0 °C) from the melt state to induce the α-phase and β-phase crystallization respectively. A significant increase by approx. one decade in the crystal/nuclei density is detected by quenching into cold water (approx. 10^7 nuclei per mm^3 *vs.* 10^6 nuclei per mm^3). Homogeneous nucleation studies were recently performed on poly(butylene terephthalate) (PBT) using various techniques such as FDSC and atomic force microscopy with a typical increase of the nuclei density by 9 decades reaching 10^{15} nuclei per mm^3 for homogeneous nucleation of PBT α-crystals.[57] In this respect, our results concerning the low temperature β-phase crystallization of PVDF seem incompatible with a homogeneous nucleation process and a heterogeneous process that involves PMMA could explain these crystal density measurements. It could be noticed here that such effects still require in-depth investigations, in particular within miscible blends where peculiar effects are observed in terms of crystallization rate.[58–60]

In an effort to gather all previous findings about the α-to-β transition in PVDF/PMMA blends by extrusion–calendering and thermocompression coupled with Flash DSC experiments, a crystal phase diagram was constructed to illustrate the impact of PMMA and the cooling rate on the crystallization of PVDF (Fig. 6). The experimental results obtained by Flash DSC are plotted wherein the initial part in Fig. 6 represents the appearance of the β-phase and the depression of the α-phase. The impact of PMMA as a β-phase promoter is here clearly identified in this diagram. For experimental results by melt processes such as extrusion–calendering and thermocompression, the cooling rate needs to be estimated. For thermocompression, a cooling rate close to 1 °C s^{-1} is obtained (the quenching time from 200 to 20 °C is estimated to be 3 min). For extrusion calendering, the quenching time is more difficult to evaluate and we estimated an approx. cooling rate of 200 °C s^{-1} based on previous studies,[47] even if significant variations of the cooling rate could be obtained at low film thicknesses. In this context, experimental results by melt processes are plotted with squares, triangles and circles for pure α-phase, α/β co-crystallization and pure β-phase respectively in Fig. 6. It could be observed that the experimental crystal observations after melt processes partially fit with Flash DSC experiments. The α-phase is mainly obtained by thermocompression (low cooling rates) for a PMMA content lower than 20 wt% and by extrusion–calendering for neat PVDF. The α/β co-crystallization is only observed for PVDF/PMMA films by extrusion–calendering at 5 and 10 wt% PMMA in accordance with Flash DSC experiments. Theoretically, the pure β-phase should be observed at high cooling rates and high PMMA contents. The crystallization of the pure β-phase is obtained for PVDF/PMMA blends with a PMMA content higher than 20 wt% PMMA for extrusion–calendering or 25 wt% by thermocompression. However, within these PMMA contents, amorphous PVDF/PMMA contents were obtained by Flash DSC and, in this context, correlations between Flash DSC and melt-processes for the crystallization of the pure polar β-phase are less accurate. Based on the FDSC analyses of PVDF/PMMA blends with a PMMA content higher than 20 wt% (ESI,† Fig. S05), it could be concluded that the polar β-phase in these PVDF/PMMA blends processed either by thermocompression or extrusion–calendering could slowly crystallize during storage at ambient temperature (hereafter called "cold-crystallization" in the crystal phase diagram).

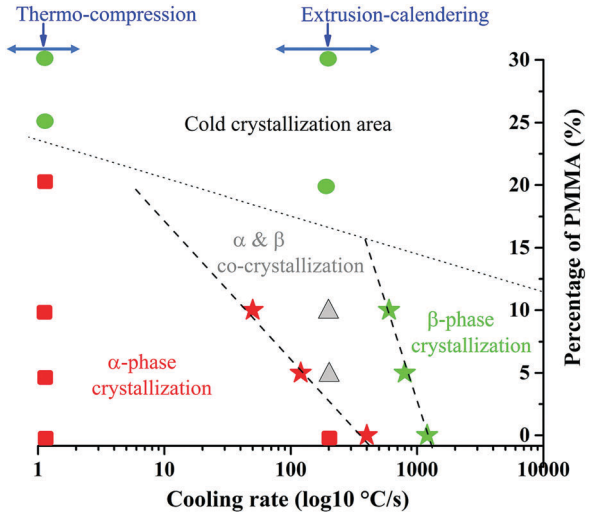

Fig. 6 Crystal phase diagram for PVDF/PMMA blends as a function of the cooling rate and weight percentage of PMMA. Experimental results by extrusion–calendering and thermocompression with pure α-phase (in red -■-), mixed α-/β-phases (grey -▲-) and pure β-phase (green -●-). Experimental results by Flash DSC are marked by stars (-*-).

This journal is © The Royal Society of Chemistry 2018

Published on 16 April 2018. Downloaded by Michigan State University on 8/13/2019 12:24:31 PM.

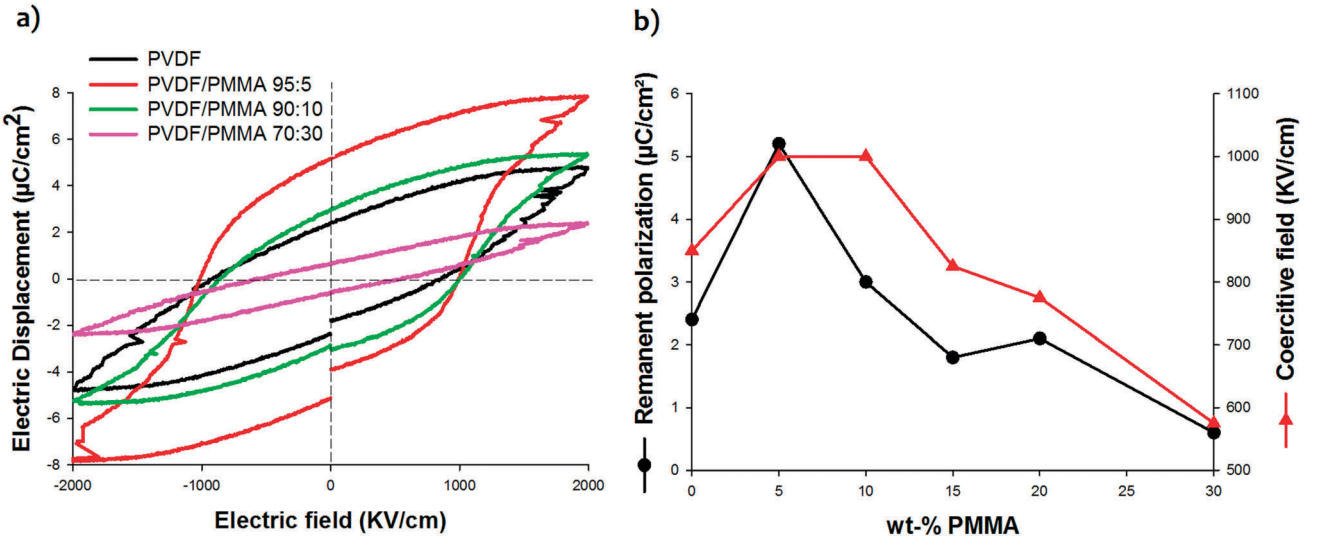

Fig. 7 Dielectric behavior for neat PVDF and PVDF/PMMA blends produced by extrusion–calendering (a) with related remanent polarization/coercive field as a function of PMMA weight content (film thickness 40 μm, maximal poling voltage 8000 V) (b).

After having confirmed the apparition of the ferroelectric/piezoelectric β-phase in the presence of PMMA by using an extrusion–calendering process with an efficient quenching, it is also of high importance to investigate the ferroelectric behavior of these as-produced PVDF/PMMA blends. For this purpose, PVDF/PMMA thin films obtained by extrusion–calendering have been characterized using a ferroelectric tester to obtain dielectric properties and potential ferroelectric properties, *i.e.* the so-called ferroelectric hysteresis loop (Fig. 7a). The samples were subjected to alternative electric fields (here a triangular waveform, see experimental section) to get information about their ferroelectric performances under high poling fields as well as correlations with the PVDF crystal structure. Therefore, neat PVDF and PVDF/PMMA films with a constant thickness of 40 μm were here subjected to alternative electric fields with a maximal electric poling field of 2000 kV cm^{-1} (corresponding to 8000 V) applied perpendicular to the film surface. Subsequent dielectric behaviors are displayed in Fig. 7a for neat PVDF and PVDF/PMMA blends with an increased PMMA weight content. Together with the shape of the hysteresis loop, two main parameters could be extracted, *i.e.*, the remanent polarization P_r (the resultant polarization after poling at high electric field) and the coercive field E_c (the electric field required to remove the polarization). Evolutions of P_r and E_c with the PMMA content are plotted in Fig. 7b. From Fig. 7a, neat PVDF does not display a well-defined pattern of ferroelectric materials[10,16,61–63] with a rather low P_r close to 2.4 μC cm^{-2}. Interestingly, by adding 5% PMMA, the dielectric response drastically changes. A clear ferroelectric behavior is obtained, as suggested by the typical squareness of the hysteresis loop and high P_r/E_c values with a 2-fold increase in the remanent polarization P_r up to 5.2 μC cm^{-2} (poling field 2000 kV cm^{-1}) (Fig. 7b). Compared to the so-called P(VDF-*co*-TrFE) (P_r close to 8.4 μC cm^{-2} at a poling field of 4000 kV cm^{-1}, and a value experimentally-verified close to 9.7 μC cm^{-2} at a poling field of 10 000 kV cm^{-1}, see ESI,† Fig. S06) and to a stretched PVDF film (P_r close to 5.5 μC cm^{-2} at a poling field of 2000 kV cm^{-1}),[64] competitive performances are concluded for our PVDF/PMMA blend with 5 wt% PMMA. This film also displays several important advantages in terms of processing and costs (no stretching is required). In this context, the enhanced β-phase content arising from the addition of 5 wt% PMMA in an extrusion–calendering process plays a major role to obtain an enhanced ferroelectric behavior without any stretching steps. However, it seems that the β-phase content does not represent the only important parameter to control the ferroelectric properties of PVDF/PMMA blends. Indeed, despite a high β-phase content, further increase of the PMMA content does not favor ferroelectric behaviors. The PVDF/PMMA blend with 10 wt% PMMA displays a similar dielectric behavior to neat PVDF (Fig. 7a) and a pseudo-linear dielectric behavior is observed at 30 wt% PMMA with poor P_r/E_c. As a conclusion, the best ferroelectric performances are obtained with the incorporation of 5 wt% PMMA and dielectric behaviors progressively switch to pseudo-linear dielectric at a higher PMMA content.

The origin of the above-mentioned transition from ferroelectric (5 wt% PMMA) to pseudo-linear dielectric behavior (30 wt% PMMA) is of high interest for further process/material optimization. It was here largely demonstrated that a quasi-pure β-phase could be obtained above 10 wt% PMMA but no ferroelectric behavior is observed for these formulations. Several phenomena could be speculated for this drastic change in dielectric behavior at high PMMA contents. In a first approach, the PVDF crystallinity (normalized to a PVDF content) remains constant in all blends but the overall crystalline content naturally decreases due to the addition of the miscible amorphous PMMA phase with a potential loss of ferroelectric properties. However, the spatial distribution of the amorphous PMMA phase could also play a key role in the resultant ferroelectric properties and the presence of PMMA in the amorphous regions of polar PVDF spherulites is suspected on the basis of (i) the difficulty to pole β-crystals at high voltages

Published on 16 April 2018. Downloaded by Michigan State University on 8/13/2019 12:24:31 PM.

and high PMMA contents as depicted in Fig. 7a with a low polarization at saturation and (ii) previous research articles pointing out the importance of the dipole coupling between PVDF crystal lamellas with complex relationships between the amount of β-crystals, their crystal size and their surrounding amorphous phase.[10,16,61–63] Strong modifications of the dielectric behavior were previously detected for PVDF-TrFE with grafted poly(methacrylates) or poly(styrene) side chains that generate relaxor/antiferroelectric-like behavior, arising from a ''nano-confinement'' effect of PVDF β-crystals.[29,61,65,66] In this context, the spatial distribution of PMMA with a potential segregation into the amorphous regions of polar PVDF spherulites was investigated by SAXS, a powerful technique to probe the crystalline morphology of semi-crystalline polymers at the lamellar level.[24,67–70] Fig. 8a displays SAXS data for various PVDF/PMMA blends produced by extrusion–calendering and a clear peak is observed for neat PVDF and all PVDF/PMMA blends for q-values in the range of 0.05–0.08. This peak is related to the regular arrangement of PVDF crystalline lamellas with its associated interlamellar amorphous phase. The long period (L_p) could be calculated from the peak position[68] and its evolution with PMMA weight content is plotted in Fig. 8b. Interestingly, L_p remains nearly constant up to 5 wt% PMMA followed by a marked and regular increase for a PMMA content higher than 10 wt%. This increase in L_p has been previously reported for numerous amorphous/semi-crystalline miscible blends (PVDF/PMMA,[24,67] PLLA/PMMA,[68] PLLA/PVPh[69] and PEO/PMMA[70]) and was largely attributed to a (partial) segregation of the amorphous component into the interlamellar amorphous phase with an increase in the intermellar distance. PMMA is consequently (partly)-trapped into the interlamellar amorphous phase of polar PVDF spherulites with a significant swelling effect on polar PVDF lamellas. The dielectric constant and the electric field across the interlamellar amorphous phase could be inherently reduced and the transition from ferroelectric to pseudo-linear dielectric behavior at a PMMA content higher than 10 wt% is consistent with a reduction of the dipole coupling between PVDF polar lamellas. As a consequence, the amount of β-crystals does not represent the only parameter controlling the final dielectric properties in PVDF/PMMA blends and a specific attention should be payed to (partial)-segregation effects of PMMA within the interlamellar amorphous phase.

Conclusions

In this study, we demonstrated that poly(methyl methacrylate) (PMMA) acts as a β-phase promoter for PVDF-based blends by melt-state processing technologies, *i.e.* extrusion–calendering and extrusion–compression. PMMA contents as low as 5 wt% are required to promote PVDF β-crystals using an extrusion–calendering technology as observed by infrared spectroscopy (FTIR) and wide-angle X-ray scattering experiments (WAXS). Flash DSC experiments definitely confirmed that the cooling rate from the melt state plays a key role with an α-to-β crystal transition at high cooling rates for neat PVDF. The incorporation of PMMA into PVDF clearly shifts this transition to lower cooling rates, *i.e.*, approx. 50–100 °C s^{-1} for 10 wt% PMMA (against 400–800 °C s^{-1} for neat PVDF), compatible with the standard processing tools of the plastic industry. A crystal phase diagram was proposed and discussed for PVDF/PMMA to highlight the synergistic effect of the PMMA content and the cooling rate on the development of PVDF β-crystals using melt-state processes. Ferroelectric properties were finally established for various PVDF/PMMA compositions and an interesting ferroelectric behavior was specifically observed for a PMMA content of 5 wt% with the highest remanent polarization. Despite a high β-phase content, the dielectric properties of PVDF/PMMA thin films with PMMA contents higher than 10 wt% progressively switched to pseudo-linear dielectric behaviors at excessive PMMA of 30 wt%. This transition seems to arise from a strong modification of the amorphous regions of PVDF polar

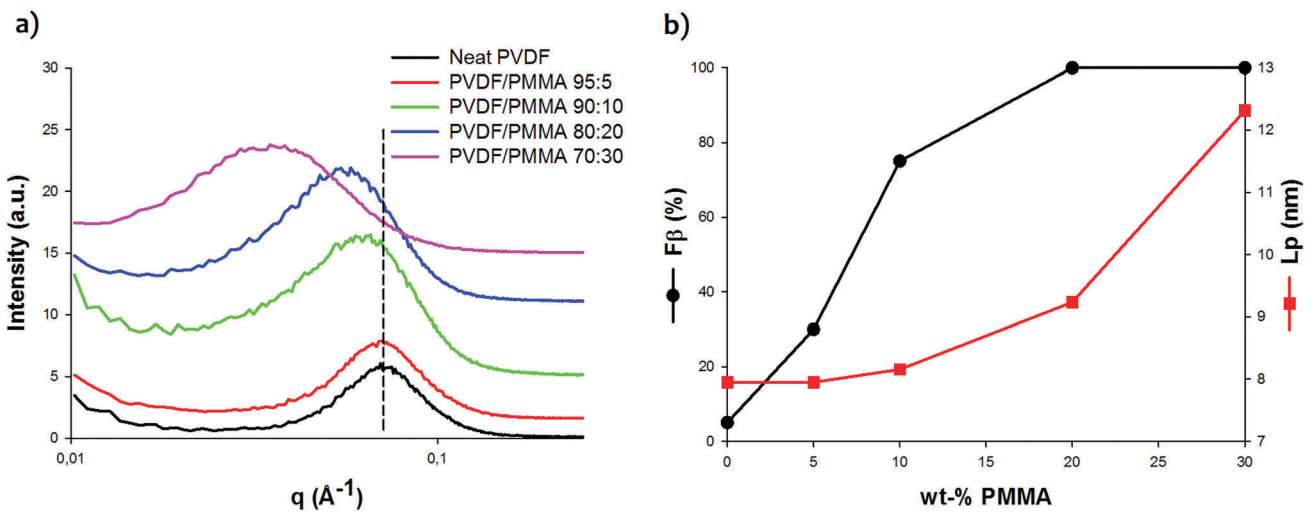

Fig. 8 SAXS analysis of neat PVDF and PVDF/PMMA films produced by extrusion–calendering (a) with related evolutions of the β-phase content (F_β) and long period (L_p) with the weight content of PMMA (b) (β-phase content measured by ATR-FTIR[2]).

 This journal is © The Royal Society of Chemistry 2018

Published on 16 April 2018. Downloaded by Michigan State University on 8/13/2019 12:24:31 PM.

spherulites in the presence of PMMA, as revealed by SAXS. Hence, PVDF/PMMA thin films made by extrusion–calendering could represent a cost-competitive route to electroactive polymer materials without the need for pre/post-treatments (*i.e.* stretching). In a forthcoming article, piezoelectric and dielectric characterization will be addressed more intensively in order to state their performances in practical applications such as actuators and/or energy harvesting applications.

Conflicts of interest

There are no conflicts to declare.

Acknowledgements

The authors gratefully acknowledge the Wallonia Region, West-Vlaanderen Region, Agentschap Innoveren Ondernemen and European Community (FEDER funds) for the financial support in the framework of the INTERREG V FWVL – BIOHARV project (GoToS3 portofolio). The authors particularly thank Samuel Devisme from Arkema for supplying raw materials. UMons – LPCM gratefully acknowledges the Belgian Federal Government Office of Science Policy (SSTC – PAI 6/27) for general support and is much indebted to both the Wallonia Region and the European Commission (FSE/FEDER) for financial support in the framework of phasing-out Hainaut. IMT Lille Douai, Université de Lille and Université de Valenciennes acknowledge both the International Campus on Safety and Intermodality in Transportation (CISIT, France), the Hauts-de-France Region (France) and the European Community (FEDER) for their contributions to funding extrusion equipment, SAXS-WAXS laboratory equipment and calorimetric/ferroelectric characterization tools.

References

1 A. Bruno, *Chem. Rev.*, 2009, **109**, 6632–6686.
2 P. Martins, A. C. Lopes and S. Lanceros-Mendez, *Prog. Polym. Sci.*, 2014, **39**, 683–706.
3 N. Murayama, K. Nakamura, H. Obara and M. Segawa, *Ultrasonics*, 1976, **14**, 15–23.
4 J. H. Jeon, S. P. Kang, S. Lee and I. K. Oh, *Sens. Actuators, B*, 2009, **143**, 357–364.
5 D. Vatansever, R. L. Hadimani, T. Shah and E. Siores, *Smart Mater. Struct.*, 2011, **20**, 55019–55024.
6 S. Das and J. Appenzeller, *Nano Lett.*, 2011, **11**, 4003–4007.
7 M. Sharma, G. Madras and S. Bose, *Macromolecules*, 2014, **47**, 1392–1402.
8 D. J. Lin, C. L. Chang, C. K. Lee and L. P. Cheng, *Eur. Polym. J.*, 2006, **42**, 2407–2418.
9 M. Li, H. J. Wondergem, M. Spijkman, K. Asadi, I. Katsouras, P. W. M. Blom and D. M. De Leeuw, *Nat. Mater.*, 2013, **12**, 1–6.
10 K. S. Ramadan, D. Sameoto and S. Evoy, *Smart Mater. Struct.*, 2014, **23**, 033001–033025.
11 B. Mohammadi, A. A. Yousefi and S. M. Bellah, *Polym. Test.*, 2007, **26**, 42–50.
12 B. R. Hahn and J. H. Wendorff, *Polymer*, 1985, **26**, 1611–1618.
13 E. Fukada, *IEEE Trans. Ultrason. Eng.*, 2000, **47**, 1277–1290.
14 V. Bharti and R. Nath, *J. Phys. D: Appl. Phys.*, 2001, **34**, 667–672.
15 V. Bharti, T. Kaura and R. Nath, *IEEE Trans. Dielectr. Electr. Insul.*, 1997, **4**, 738–741.
16 L. Zhu, *J. Phys. Chem. Lett.*, 2014, **5**, 3677–3687.
17 M. Li, N. Stingelin, J. J. Michels, M.-J. Spijkman, K. Asadi, K. Feldman, P. W. M. Blom and D. M. de Leeuw, *Macromolecules*, 2012, **45**, 7477–7485.
18 A. Lund, C. Gustafsson, H. Bertilsson and R. W. Rychwalski, *Compos. Sci. Technol.*, 2011, **71**, 222–229.
19 S. Mishra, K. T. Kumaran, R. Sivakumaran, S. P. Pandian and S. Kundu, *Colloids Surf., A*, 2016, **509**, 684–696.
20 K. Ke, P. Pötschke, D. Jehnichen, D. Fischer and B. Voit, *Polymer*, 2014, **55**, 611–619.
21 L. L. Sun, B. Li, Z. G. Zhang and W. H. Zhong, *Eur. Polym. J.*, 2010, **46**, 2112–2119.
22 V. Sencadas, S. Lanceros-Méndez and J. F. Mano, *Thermochim. Acta*, 2004, **424**, 201–207.
23 H. Sasaki, P. Kanti Bala, H. Yoshida and E. Ito, *Polymer*, 1995, **36**, 4805–4810.
24 Y. Okabe, H. Murakami, N. Osaka, H. Saito and T. Inoue, *Polymer*, 2010, **51**, 1494–1500.
25 A. Linares and J. L. Acosta, *Eur. Polym. J.*, 1997, **33**, 467–473.
26 C. Léonard, J. L. Halary and L. Monnerie, *Macromolecules*, 1988, **21**, 2988–2994.
27 C. Domenici, D. De Rossi, A. Nannini and R. Verni, *Ferroelectrics*, 1984, **60**, 61–70.
28 S. J. Kang, Y. J. Park, I. Bae, K. J. Kim, H. C. Kim, S. Bauer, E. L. Thomas and C. Park, *Adv. Funct. Mater.*, 2009, **19**, 2812–2818.
29 J. Li, X. Hu, G. Gao, S. Ding, H. Li, L. Yang and Z. Zhang, *J. Mater. Chem. C*, 2013, **1**, 1111–1121.
30 R. Androsch and M. L. Di Lorenzo, *Macromolecules*, 2013, **46**, 6048–6056.
31 J. E. K. Schawe, *Thermochim. Acta*, 2015, **603**, 85–93.
32 Y. Chen, X. Chen, D. Zhou, Q. D. Shen and W. Hu, *Polymer*, 2016, **84**, 319–327.
33 A. Gradys, P. Sajkiewicz, S. Adamovsky, A. Minakov and C. Schick, *Thermochim. Acta*, 2007, **461**, 153–157.
34 C. Samuel, S. Barrau, J.-M. Lefebvre, J.-M. Raquez and P. Dubois, *Macromolecules*, 2014, **47**, 6791–6803.
35 M. Leveque, C. Douchain, M. Rguiti, K. Prashantha, C. Courtois, M. F. Lacrampe and P. Krawczak, *Int. J. Polym. Anal. Charact.*, 2016, **22**, 1–26.
36 S. Charlon, S. Marais, E. Dargent, J. Soulestin, M. Sclavons and N. Follain, *Phys. Chem. Chem. Phys.*, 2015, **44**, 29918–29934.
37 G. M. Sessler, *J. Acoust. Soc. Am.*, 1981, **70**, 1596–1608.
38 A. Salimi and A. A. Yousefi, *Polym. Test.*, 2003, **22**, 699–704.
39 M. Veitmann, D. Chapron, S. Bizet, S. Devisme, J. Guilment and I. Royaud, *Polym. Test.*, 2015, **48**, 120–124.
40 L.-Z. Liu, B. Chu, J. P. Penning and R. S. J. Manley, *Macromolecules*, 1997, **30**, 4398–4404.
41 R. Gregorio Jr and N. C. P. de Souza Nociti, *J. Phys. D: Appl. Phys.*, 1995, **28**, 432–436.

Published on 16 April 2018. Downloaded by Michigan State University on 8/13/2019 12:24:31 PM.

42 S. Schneider, X. Drujon, J. Wittmann and B. Lotz, *Polymer*, 2001, **42**, 8799–8806.
43 J. W. Park, Y. A. Seo, I. Kim, C. S. Ha, K. Aimi and S. Ando, *Macromolecules*, 2004, **37**, 429–436.
44 S. I. Oioscoi, K. Jin, Y. Ju and Y. Ho, *Vib. Spectrosc.*, 1995, **9**, 147–159.
45 D. Yang and Y. Chen, *J. Mater. Sci. Lett.*, 1987, **6**, 599–603.
46 V. Tiwari and G. Srivastava, *J. Polym. Res.*, 2014, **21**, 587.
47 R. Ali, S. Iannace and L. Nicolais, *Compos. Sci. Technol.*, 2003, **63**, 2217–2222.
48 A. Toda, R. Androsch and C. Schick, *Polymer*, 2016, **91**, 239–263.
49 E. Zhuravlev, J. W. P. Schmelzer, B. Wunderlich and C. Schick, *Polymer*, 2011, **52**, 1983–1997.
50 R. Androsch, H. M. N. Iqbal and C. Schick, *Polymer*, 2015, **81**, 151–158.
51 Y. Chen, Q. D. Shen and W. Hu, *Polym. Int.*, 2016, **65**, 387–392.
52 A. Gradys, P. Sajkiewicz, E. Zhuravlev and C. Schick, *Polymer*, 2016, **82**, 40–48.
53 W.-K. Lee and C.-S. Ha, *Polymer*, 1998, **39**, 7131–7134.
54 B. R. Hahn, O. Herrmann-Schönherr and J. H. Wendorff, *Polymer*, 1987, **28**, 201–208.
55 E. Freire, O. Bianchi, E. E. C. Monteiro, R. C. Reis Nunes and M. C. Forte, *Mater. Sci. Eng., C*, 2009, **29**, 657–661.
56 I. Kolesov, D. Mileva, R. Androsch and C. Schick, *Polymer*, 2011, **52**, 5156–5165.
57 R. Androsch, A. M. Rhoades, I. Stolte and C. Schick, *Eur. Polym. J.*, 2015, **66**, 180–189.
58 C. Samuel, J. Cayuela, I. Barakat, A. J. Müller, J. M. Raquez and P. Dubois, *ACS Appl. Mater. Interfaces*, 2013, **5**, 11797–11807.
59 Z. Bartczaka and E. Martuscelli, *Macromol. Chem. Phys.*, 1987, **188**, 445–453.
60 M. L. Addonizio, E. Martuscelli and C. Silvestre, *Polymer*, 1987, **28**, 183–188.
61 L. Zhu and Q. Wang, *Macromolecules*, 2012, **45**, 2937–2954.
62 M. Kanik, O. Aktas, H. S. Sen, E. Durgun, M. Bayindir and M. Science, *ACS Nano*, 2014, **8**, 9311–9323.
63 J. Wei, Z. Zhang, J. K. Tseng, I. Treufeld, X. Liu, M. H. Litt and L. Zhu, *ACS Appl. Mater. Interfaces*, 2015, **7**, 5248–5257.
64 M. Mackey, D. E. Schuele, L. Zhu, L. Flandin, M. A. Wolak, J. S. Shirk, A. Hiltner and E. Baer, *Macromolecules*, 2012, **45**, 1954–1962.
65 J. Li, S. Tan, S. Ding, H. Li, L. Yang and Z. Zhang, *J. Mater. Chem.*, 2012, **22**, 23468.
66 M. Neidhöfer, F. Beaume, L. Ibos, A. Bernès and C. Lacabanne, *Polymer*, 2004, **45**, 1679–1688.
67 H. Saito and B. Stühn, *Macromolecules*, 1994, **27**, 216–218.
68 M. Canetti, A. Cacciamani and F. Bertini, *J. Polym. Sci., Part B: Polym. Phys.*, 2014, **52**, 1168–1177.
69 H. L. Chen, H. H. Liu and J. S. Lin, *Macromolecules*, 2000, **33**, 4856–4860.
70 T. P. Russell, H. Ito and G. D. Wignall, *Macromolecules*, 1988, **21**, 1703–1709.

 This journal is © The Royal Society of Chemistry 2018